J|A|C|S
ARTICLES
Published on Web 04/12/2002

Effects of Thioamide Substitutions on the Conformation and Stability of α- and 3_{10}-Helices

Tran Trung Tran,[†] Jun Zeng,[‡] Herbert Treutlein,[‡] and Antony W. Burgess*

Contribution from the Ludwig Institute for Cancer Research and Cooperative Research Centre for Cellular and Growth Factors, Melbourne, Victoria, 3050, Australia

Received August 8, 2001. Revised Manuscript Received November 2, 2001

Abstract: Thiopeptides, formed by replacing the amide oxygen atom with a sp^2 sulfur atom, are useful in protein engineering and drug design because they confer resistance to enzymatic degradation and are predicted to be more rigid. This report describes our free molecular dynamics simulations with explicit water and free energy calculations on the effects of thio substitutions on the conformation of α-helices, 3_{10}-helices, and their relative stability. The most prominent structural effect of thio substitution is the increase in the hydrogen bond distance from 2.1 Å for normal peptides to 2.7 Å for thiopeptides. To accommodate for the longer C═S···H−N hydrogen bond, the (ϕ, ψ) dihedral angles of the α-helix changed from (−66°, −42°) to (−68°, −38°), and the rise per turn increased from 5.5 to 6.3 Å. For 3_{10}-helices, the (ϕ, ψ) dihedral angles (−60°, −20°) and rise per turn (6.0 Å) changed to (−66°, −12°) and 6.8 Å, respectively. In terms of relative stability, the most prominent change upon thio substitution is the decrease in the free energy difference, $\Delta A(\alpha \rightarrow 3_{10})$, from 14 to 3.5 kcal/mol. Therefore, normal peptides are less likely to form 3_{10}-helix than are thiopeptides. Component analysis of the $\Delta A(\alpha \rightarrow 3_{10})$ reviews that the entropy advantage of the 3_{10}-helix for both Ac−Ala_{10}−NHMe and Act−$Alat_{10}$−NHMe is attributed to the 3_{10}-helix being more flexible than the α-helix. Interestingly, upon thio substitution, this differential flexibility is even more apparent because the α-helix conformation of Act−$Alat_{10}$−NHMe becomes more rigid due to the bulkier sulfur atom.

Introduction

Although the 20 amino acids encoded in the genome can be used to produce a large diversity of peptides, the use of noncoding amino acids can increase this diversity and therefore can potentially enhance protein engineering and drug discovery projects. Noncoding amino acids have also been used to restrict the conformational space of peptides,[1−3] allowing more predictable peptide conformers to be constructed with potential increase in binding affinity.[4,5] Furthermore, noncoding amino acids have been used to confer resistance to enzymatic degradation within the body,[6−8] to probe protein structures,[9−11] in *de novo* design of protein,[1,12−16] to design structures with novel fold or secondary structure,[17,18] and to create new combinatorial chemistry libraries.[19−24] When the oxygen of the peptide unit is replaced by a sp^2 sulfur atom, the thiopeptide formed becomes resistant to enzymatic degradation.[7,8] Thiopeptides have been used in structure activity relationship studies to alter biological activities,[6,25−27] and, in particular, a thio-enkephalin has been

* To whom correspondence should be addressed. Tel.: (+613) 9341-3155. Fax: (+613) 9341-3104. E-mail: Tony.Burgess@ludwig.edu.au.

[†] Current address: Institute of Molecular Bioscience, University of Queensland, Brisbane, QLD, 4072, Australia.

[‡] Current address: Cytopia PTY. LTD, 7th Floor Daly Wing, St. Vincent's Hospital, 41, Victoria Parade, Fitzroy, Victoria 3065, Australia.

(1) Prasad, B. V. V.; Balaram, P. *Crit. Rev. Biochem.* **1983**, *16* (4), 307−348.
(2) Aubury, A.; Protas, J.; Boussard, G.; Marraud, M.; Neel, J. *Biopolymers* **1978**, *17*, 1693−1711.
(3) Paterson, Y.; Rumsey, S. M.; Benedetti, E.; Nemethy, G.; Scheraga, H. A. *J. Am. Chem. Soc.* **1981**, *103*, 2947−2955.
(4) Veber, D. F.; Freidinger, R. M.; Perlow, D. S.; Paleveda, W. J.; Holly, F. W.; Strachan, R. G.; Nutt, R. F.; Arison, B. H.; Homnick, C.; Randall, W. C.; Glitzer, M. S.; Saperstein, R.; Hirschmann, R. *Nature* **1981**, *292*, 55−58.
(5) Veber, D. F.; Holly, F. W.; Nutt, R. F.; Bergstrand, S. J.; Brady, S. F.; Hirschmann, R. *Nature* **1979**, *280*, 512−514.
(6) Spatola, A. F. *Chemistry and Biochemistry of Amino Acids, Peptides, and Proteins*; Dekker: New York, 1983; pp 267−357.
(7) Michel, A. G.; Ameziane-Hassani, C.; Boulay, G. *Can. J. Chem.* **1989**, *67*, 1312−1318.
(8) Mock, W. L.; Chen, J. T.; Tsang, J. W. *Biochem. Biophys. Res. Commun.* **1981**, *102*, 389−396.
(9) Rutledge, L. D.; Perlman, J. H.; Gershengorn, M. C.; Marshall, G. R.; Moeller, K. D. *J. Med. Chem.* **1996**, *39* (8), 1571−1574.
(10) Juvvadi, P.; Dooley, D. J.; Humblet, C. C.; Lu, G. H.; Lunney, E. A.; Panek, R. L.; Skeean, R.; Marshall, G. R. *Int. J. Pept. Protein Res.* **1992**, *40*, 163−170.
(11) Turk, J.; Marshall, G. R. *Biochemistry* **1975**, *14*, 2631−2635.
(12) Karle, I. L.; Flippen-Anderson, J. L.; Sukumar, M.; Uma, K.; Balaram, P. *J. Am. Chem. Soc.* **1991**, *113*, 3952−3956.
(13) Degrado, W. F.; Raleigh, D. P.; Handel, T. *Curr. Opin. Struct. Biol.* **1991**, *1*, 984−993.
(14) Burgess, A. W.; Leach, S. J. *Biopolymers* **1973**, *12*, 2599−2605.
(15) Marshall, G. R.; Bosshard, H. A. *Circ. Res.* **1972**, *30/31(Supp. II)*, 143.
(16) Ramnarayan, K.; Chan, M. F.; Balaji, V. N.; Profeta, S., Jr.; Rao, S. N. *Int. J. Pept. Protein Res.* **1995**, *45*, 366−376.
(17) Apella, D. H.; Christianson, L. A.; Karle, I. L.; Powell, D. R.; Gellman, S. H. *J. Am. Chem. Soc.* **1996**, *118*, 13071−13072.
(18) Seebach, D.; Overhand, M.; Kuhnle, F. N. M.; Martinoni, B.; Oberer, L.; Hommel, U.; Wdimer, H. *Helv. Chim. Acta* **1996**, *79*, 913−941.
(19) Simon, R. J.; Kania, R. S.; Zuchermann, R. N.; Huebner, V. D.; Jewell, D. A.; Banville, S.; Ng, S.; Wang, L.; Rosenberg, S.; Marlowe, C. K. *Proc. Natl. Acad. Sci. U.S.A.* **1992**, *89*, 9367−9371.
(20) Kassler, H. *Angew. Chem., Int. Ed. Engl.* **1993**, *32*, 543−544.
(21) Zuchermann, R. N.; Kerr, J. M.; Kent, S. B. H.; Moos, W. H. *J. Am. Chem. Soc.* **1992**, *114*, 10646−10647.
(22) Zuchermann, R. N.; Martin, E. J.; Spellmeyer, D. C.; Stauber, G. B.; Shoemaker, K. R.; Kerr, J. M.; Figliozzi, G. M.; Goff, D. A.; Siani, M. A.; Simon, R. J. *J. Med. Chem.* **1994**, *37*, 2678−2685.
(23) Miller, S. M.; Simon, R. J.; Ng, S.; Zuchermann, R. N.; Kerr, J. M.; Moos, W. H. *Drug Dev. Res.* **1995**, *35*, 20−32.
(24) Allinger, N. L.; Chen, K.; Lii, J.-H. *J. Comput. Chem.* **1996**, *17*, 642−668.

10.1021/ja011916o CCC: $22.00

Table 1. $\Delta G(\alpha \rightarrow 3_{10})$ for Polyalanine and PolyAib Calculated by Other Authors

system	$\Delta G(\alpha \rightarrow 3_{10})$ kcal/mol	ΔU	$-t\Delta S_{tot}$	reference
Ac−Ala_{10}−NHMe (in vacuo)	8	12	−4	Zhang et al.[46]
Ac−Ala_{10}−NHMe (water)	16			Zhang et al.[46]
Ac−Ala_{11}−NHMe (in vacuo)	13.4			Tirado-Rives et al.[45]
Ac−Ala_{11}−NHMe (water)	10.5			Tirado-Rives et al.[45]
Ac−Aib_{10}−NHMe (in vacuo)	−4.3	0	−4.3	Zhang et al.[46]
Ac−Aib_{10}−NHMe (water)	0.1			Zhang et al.[46]
Ac−Aib_{10}−NHMe (in vacuo)	3.2 ± 0.8	4.4 ± 1.2	-1.2 ± 0.4	Smythe et al.[47,54]
Ac−Aib_{10}−NHMe (water)	7.6 ± 0.4	12 ± 5	-4 ± 5	Smythe et al.[47,54]

shown to have enhanced potency and a change in selectivity in both biological and binding assays.[26] Our previous X-ray studies[28] and conformational energy and free energy calculations of thio substituted dipeptides[29−32] suggest they are more conformationally restricted than peptides and have distinctly different hydrogen bonding properties.

Most amino acids in peptides and proteins are part of secondary structure elements: 35% of all residues are found in α- or 3_{10}-helices,[33] 25% of residues are found in *β*-turns,[34] and 20% of residues are found in *β*-sheets.[35] Apart from the fact that α- and 3_{10}-helices constitute a high percentage of all the residues in proteins and peptides, the relative stability of these structures can be important to substrate binding.[36,37] 3_{10}-Helices have been implicated in the stabilization of the α-helix ends[38,39] and may be an intermediate in the folding/unfolding α-helices.[40−44] Tirado-Rives et al.[45] calculated the relative free energy $\Delta G(\alpha \rightarrow 3_{10})$ for the conversion of Ac−Ala_{11}−NHMe from α-helix to 3_{10}-helix. The $\Delta G(\alpha \rightarrow 3_{10})$ was found to be 10.5 kcal/mol in water and 13.4 kcal/mol in vacuo (see Table 1). They decomposed the intramolecular energy (ΔH_{uu}) of Ac−Ala_{11}−NHMe into angle, torsion, and nonbonded components and concluded that the 3_{10}-helix is intrinsically less stable because of the higher nonbonded interactions energy. Zhang and Herman[46] used the slow growth method to calculate the $\Delta G(\alpha \rightarrow 3_{10})$ for both Ac−Ala_{10}−NHMe and Ac−Aib_{10}−NHMe in explicit water. The α-helical conformation of Ac−Ala_{10}−NHMe was 16 kcal/mol more stable than the 3_{10}-helical conformation, whereas the α- and 3_{10}-helical conformations of Ac−Aib_{10}−NHMe appear to be equally probable (see Table 1). Finally, the free energy profile of a 3_{10}- to α-helix transition for Ac−Aib_{10}−NHMe has been simulated by Smythe et al.[47] using molecular dynamic simulations. These calculations indicated that the α-helix is more stable in comparison to the 3_{10}-helix by about 7.6 kcal/mol in water and 3.3 kcal/mol in vacuo (Table 1).

In this report, we present the calculation of the Helmholtz free energy difference between the α-helical and the 3_{10}-helical conformation, $\Delta A(\alpha \rightarrow 3_{10})$, for polyalanine in explicit water environment. The free energy differences were decomposed into enthalpy and entropy components. The enthalpy components were divided into peptide−peptide and peptide−water components, which were further subdivided into electrostatics, van der Waals, and internal components. It should be noted that Tirado-Rives et al.[45] only performed partial decomposition, Zhang and Herman's[46] free energy decomposition was for in vacuo simulation, and the Smythe et al.[47] calculations are on Ac−Aib_{10}−NHMe. Furthermore, we have calculated, for the first time, the α- and 3_{10}-helix conformations of polythioalanine, as well as their relative stability in an explicit water environment and its decomposition into enthalpy and entropy components.

Methods

Unless stated otherwise, all the molecular dynamic simulations in this paper were performed using the CDiscover[48] program with constant volume, periodic boundary conditions, and 1 fs time step. The temperature was kept at 298 K with a window of 10 K, beyond which temperature control was activated. Temperature was controlled by "Velocity Scaling" and integrated by the method of "Velocity Verlet".[48,49] A group-based cutoff distance of 15 Å was used with a spline width of 1 Å and a buffer width of 0.5 Å.

Simulation of the α-Helical Conformation of Polyalanine and Polythioalanine. The InsightII program was used to place Ac−Ala_{24}−NHMe in a rectangular unit cell with cell dimensions of $a = 53$ Å, $b = 26$ Å, $c = 26$ Å, and $\alpha = \beta = \gamma = 90°$. The unit cell was filled with 1092 water molecules to produce a density of approximately 1 g/cm^3. Act−$Alat_{24}$−NHMe was placed in a slightly longer box ($57 \times 26 \times 26$ Å) of water to accommodate the longer peptide. The initial ϕ and ψ dihedral angles for the α-helix conformations were set to the most favorable angles observed in the implicit water molecular dynamics calculations. After the equilibration, molecular dynamics simulations were performed for 120 ps.

Simulation of the 3_{10}-Helical Conformation of Polyalanine and Polythioalanine. For simulation of 3_{10}-helical structures, the shorter peptides Ac−Ala_{10}−NHMe and Act−$Alat_{10}$−NHMe were used. The peptides were placed in their individual unit cell ($36 \times 22 \times 22$ Å),

(25) Yde, B.; Thomsen, I.; Thorsen, M.; Clausen, K.; Lawesson, S.-O. *Tetrahedron* **1983**, *39*, 4121−4126.
(26) Clausen, K.; Spatola, A. F.; Lemieux, C.; Schiller, P. W.; Lawesson, S.-O. *Biochem. Biophys. Res. Commun.* **1984**, *120*, 305−310.
(27) Jones, W. C., Jr.; Nestor, J. J., Jr.; Vigneaud, V. d. *J. Am. Chem. Soc.* **1973**, *95*, 5677−5679.
(28) Tran, T. T.; Treutlein, H. R.; Burgess, A. W.; Perich, J. *J. Pept. Res.* **2001**, *58*, 67−78.
(29) La Cour, T. F. M. *Int. J. Pept. Protein Res.* **1987**, *30*, 564−571.
(30) Tran, T. T.; Treutlein, H. R.; Burgess, A. W. *J. Comput. Chem.* **2001**, *22*, 1010−1025.
(31) Tran, T. T.; Treutlein, H. R.; Burgess, A. W. *J. Comput. Chem.* **2001**, *22*, 1026−1037.
(32) Tran, T. T.; Burgess, A. W.; Treutlein, H. R.; Zeng, J. *J. Mol. Graphics Modell.* **2001**, *20*, 245−256.
(33) Barlow, D. J.; Thornton, J. M. *J. Mol. Biol.* **1988**, *201*, 601−619.
(34) Wilmot, C. M.; Thornton, J. M. *J. Mol. Biol.* **1988**, *203*, 221−232.
(35) Toniolo, C. *Crit. Rev. Biochem.* **1980**, *9*, 1−44.
(36) Gerstein, M.; Chothia, C. *J. Mol. Biol.* **1991**, *220*, 133−139.
(37) McPhalen, C. A.; Vincent, M. G.; Picot, D.; Jansonius, J. N.; Lesk, A. M.; Chothia, C. *J. Mol. Biol.* **1992**, *227*, 197−213.
(38) Fiori, W. R.; Miick, S. M.; Millhauser, G. L. *Biochemistry* **1993**, *32*, 11957−11962.
(39) Millhauser, G. L. *Biochemistry* **1995**, *34*, 3873−3877.
(40) Sundaralingam, M.; Sekharudu, Y. C. *Science* **1989**, *244*, 1333−1337.
(41) Tobias, D. J.; Brooks, C. L., III. *Biochemistry* **1991**, *30*, 6059−6070.
(42) Soman, K. V.; Karimi, A.; Case, D. A. *Biopolymers* **1991**, *31*, 1351−1361.
(43) Tirado-Rives, J.; Jorgensen, W. L. *Biochemistry* **1991**, *30*, 3964−3871.
(44) Hirst, J. D.; Brooks, C. L., III. *Biochemistry* **1995**, *34*, 7614−7621.
(45) Tirado-Rives, J.; Maxwell, D. S.; Jorgensen, W. L. *J. Am. Chem. Soc.* **1993**, *115*, 11590−11593.
(46) Zhang, L.; Hermans, J. *J. Am. Chem. Soc.* **1994**, *116*, 11915−11921.
(47) Smythe, M. L.; Huston, S. E.; Marshall, G. R. *J. Am. Chem. Soc.* **1993**, *115*, 11594−11595.
(48) *Discover 2.9.5/94.0, User Guide, Part I*; Biosym Technologies: San Diego, CA, 1994.
(49) *Discover 2.9.7/95.0/3.00. Force field simulations, User Guide, Part I*; Molecular Simulation: San Diego, California, 1995.

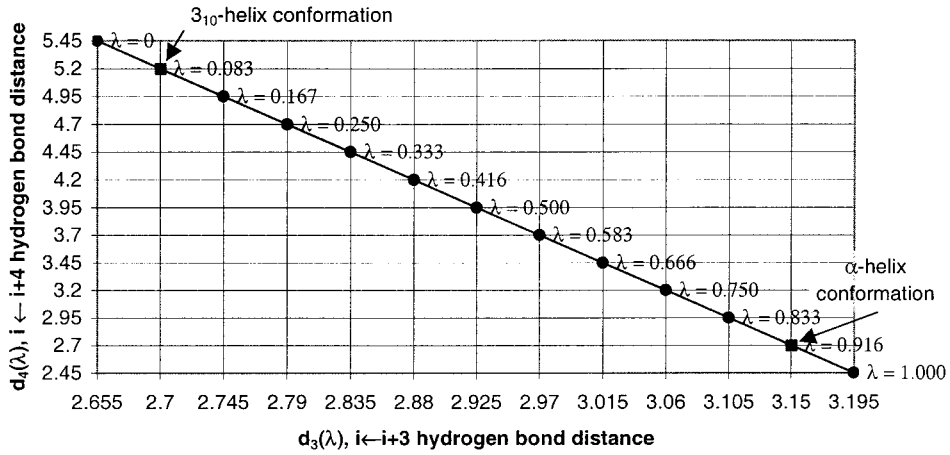

Figure 1. Reaction coordinate for Ac−Ala$_{10}$−NHMe 3$_{10}$-helix → α-helix transition.

which was filled with water molecules to produce a density of approximately 1 g/cm^3. The ϕ and ψ dihedral angles were initially set to the standard value for 3$_{10}$-helix conformation of peptides[33] (−71°, −18°). During the 15 ps equilibration period, restraints were applied to the hydrogen bond distances to keep them close to the 3$_{10}$-helical structures. After the equilibration, all restraints were removed, and free molecular dynamics simulations were performed for 120 ps.

Relative Free Energy Differences between 3$_{10}$-Helix and α-Helix for Ac−Ala$_{10}$−NHMe and Act−Alat$_{10}$−NHMe. Reaction Pathways and Biasing Functions for Umbrella Sampling. The $i \leftarrow i + 3$ and $i \leftarrow i + 4$ hydrogen bond distances were used as a reaction coordinate to connect the α- and 3$_{10}$-helices. Consequently, each Ac−Ala$_{10}$−NHMe and Act−Alat$_{10}$−NHMe molecule has nine $i \leftarrow i + 3$ hydrogen bond distance restraints and eight $i \leftarrow i + 4$ hydrogen bond distance restraints. This hydrogen bond distance reaction coordinate is less restrictive than the ϕ and ψ dihedral angles reaction coordinate used by Tirado-Rives et al.[45] From the contour map of $1 \leftarrow 3$ hydrogen bond length versus ϕ and ψ dihedral angle, we see that several sets of dihedral angles generate identical hydrogen bond distances, but there is only one hydrogen bond distance for a particular set of dihedral angles (http://www.ludwig.edu.au/archive/tran).

The following definitions were used: d_4 as the $i \leftarrow i + 4$ hydrogen bond distance, d_3 as the $i \leftarrow i + 3$ hydrogen bond distance, $d_4(\lambda)$ as the target of $i \leftarrow i + 4$ hydrogen bond restraints at window λ, and $d_3(\lambda)$ as the target of $i \leftarrow i + 3$ hydrogen bond restraints at window λ.

Four simulations were performed: two for polyalanine, (α → 3$_{10}$) and the reverse (3$_{10}$ → α), and two for polythioalanine, (α → 3$_{10}$) and the reverse (3$_{10}$ → α). For each simulation, 13 windows were sampled with λ values of 0.000, 0.083, 0.166, 0.250, 0.333, 0.416, 0.500, 0.583, 0.666, 0.750, 0.833, 0.916, and 1.000. The reaction coordinate for the (3$_{10}$ → α) polythioalanine simulation is illustrated in Figure 1. The $\lambda = 0.083$ window corresponds to the 3$_{10}$-helix conformation, and the $\lambda = 0.916$ window corresponds to the α-helix conformation.

The restraining or weighting function $W(\lambda)$ used to bias the sampling along the reaction coordinate is defined as

$$W(\lambda) = K[\sum_{\substack{i<-i+3 \\ \text{hbonds}}} (d_3 - d_3(\lambda))^2 - \sum_{\substack{i<-i+4 \\ \text{hbonds}}} (d_4 - d_4(\lambda))^2]$$

where

$$d_3(\lambda) = (1 - \lambda)d_3(0) + \lambda d_3(1)$$

$$d_4(\lambda) = (1 - \lambda)d_4(0) + \lambda d_4(1)$$

From the 3$_{10}$- and α-helical conformations determined earlier, we determined the values for $d_3(\lambda = 3_{10})$, $d_4(\lambda = 3_{10})$, $d_3(\lambda = \alpha)$, and $d_4(\lambda = \alpha)$, from which we calculated $d_3(0)$, $d_3(1)$, $d_4(0)$, and $d_4(1)$. A force constant of 5 kcal mol^{-1} Å^{-2} was used. For each of the windows, after 15 ps of equilibration, molecular dynamic simulations were performed for 100 ps using a group-based cutoff of 10 Å.

Probability Distributions. Although the d_3 and d_4 values for each conformation were restrained to $d_3(\lambda)$ and $d_4(\lambda)$, respectively, the actual distances calculated from the molecular coordinates vary along each trajectory. For each restraint and each conformation in the trajectory, λ is obtained using eqs 1 and 2:

$$\text{for } i \leftarrow i + 3 \text{ hydrogen bond restraints:} \quad \lambda = \frac{d_3 - d_3(0)}{d_3(1) - d_3(0)} \quad (1)$$

$$\text{for } i \leftarrow i + 4 \text{ hydrogen bond restraints:} \quad \lambda = \frac{d_4 - d_4(0)}{d_4(1) - d_4(0)} \quad (2)$$

The λ for each conformation is obtained by averaging over the λ for that conformation. The λ values are divided into bins of width 0.005. The probability of a particular bin and of a particular restraint p_w(bin, restraint) were obtained by counting over all conformations where the value λ corresponds to the range in the bin.

Free Energy Profiles. The probability distributions above are biased by the restraining function $W(\lambda)$. The bias effects were removed by the procedure of Torrie and Valleau.[50] Because there were few restraints, the relative free energy $A(\lambda)$ is defined as

$$A(\lambda) = \sum_{\text{restraints}} [-k_B T \ln P_W(\lambda,\text{restraint}) - W(\lambda,\text{restraint})] + \text{constant} \quad (3)$$

All the calculations above were implemented in the C program analysis.c located at http://www.ludwig.edu.au/archive/tran. The relative free energies $A(\lambda)$ were determined for each window to within an additive constant to neighboring windows (see eq 3). In this study, the λ value that corresponds to the maximum overlap of adjacent probability curves is determined, then the $A(\lambda)$ curves for adjacent windows are made continuous by superimposing the $A(\lambda)$ values in the interval of three points above and three points below the λ with maximum overlap.

Thermodynamic Decomposition. To understand the free energy map in terms of microscopic interactions, the Helmholtz free energy differences (ΔA) were decomposed into their entropic (ΔS) and potential energy (ΔU) components.[51] The entropic and energetic components could be further divided into peptide−peptide (uu), peptide−water (uv), and water−water (vv) components.[51] Yu and Karplus[52] have concluded that the water−water energy contribution (ΔU_{vv}) and the entropic contribution (ΔS_{vv}) exactly cancel for each conformation. As a result,

(50) Torrie, G. M.; Valleau, J. P. *J. Comput. Phys.* **1977**, *23*, 187−199.
(51) Tobias, D. J.; Brooks, C. L., III. *J. Phys. Chem.* **1992**, *96*, 3864−3870.
(52) Yu, H.-A.; Karplus, M. *J. Chem. Phys.* **1988**, *89*, 2366−2379.

Table 2. Key Parameters for the α_R-Helix of Ac−Ala_{24}−NHMe and Act−$Alat_{24}$−NHMe Obtained from Molecular Dynamics Simulations

	Ac–Ala_{24}–NHMe	Act–$Alat_{24}$–NHMe
H-bond pattern	$i \leftarrow i + 4$	$i \leftarrow i + 4$
Φ	−66°	−68°
Ψ	−42°	−38°
H-bond distance (Å)	2.1	2.7
residue/turn	3.6	3.7
rise/turn (Å)	5.5	6.3

the relative free energy becomes

$$\Delta A = \Delta U_{uu} + \Delta U_{uv} - T(\Delta S_{uu} + \Delta S_{uv})$$

Furthermore, each of the energy components could be subdivided into van der Waals, electrostatic, and internal components. The free energy difference between the 3_{10}- and the α-helix for Ac−Ala_{10}−NHMe and Act−$Alat_{10}$−NHMe was decomposed into the different components. The ΔU_{uu} and ΔU_{uv} components and their subdivisions into electrostatic, van der Waals, and internal components were obtained from the trajectories for the 3_{10}- and the α-helix conformations (window 2 or window 12) of each potential of mean force. The entropic component $-T(\Delta S_{uu} + \Delta S_{uv})$ was calculated by subtracting the energy components from the free energy. We did not decompose the entropy into individual $-T\Delta S_{uu}$ and $-T\Delta S_{uv}$ components, so the discussion on the entropy below is based on the $-T(\Delta S_{uu} + \Delta S_{uv})$ term.

Results

α-Helical Conformations of Ac−Ala_{24}−NHMe and Act−$Alat_{24}$−NHMe. Free molecular dynamics simulations were performed for both Ac−Ala_{24}−NHMe and Act−$Alat_{24}$−NHMe in explicit water. To reduce the complication of the end-effects caused by the hydrogen bonds at the C and N terminals, only hydrogen bonds between O_{9-12} and H_{13-16} were analyzed. Furthermore, only the fluctuations in the ϕ and ψ dihedral angles between residues 10−15 were analyzed in detail. The variation of ϕ and ψ dihedral angles and hydrogen bond distances with simulation time as well as their frequency distributions were plotted (http://www.ludwig.edu.au/archive/tran). The ϕ and ψ dihedral angles and the hydrogen bond distances fluctuate widely with no obvious trend to move away from the equilibrated structure in the plot; therefore, the structure must be in a local energy minimum. Furthermore, the smoothness of the frequency plots indicates that the data was sufficiently sampled during the simulation. The most probable hydrogen bond distances for the α_R conformer of Ac−Ala_{24}−NHMe and Act−$Alat_{24}$−NHMe are 2.15 and 2.75 Å, respectively, and the most probable (ϕ, ψ) dihedral angles are (−66°, −42°) and (−68°, −38°), respectively (Table 2). The most probable α_R conformer was obtained by energy minimization with the ϕ, ψ dihedral angles and the $i \leftarrow i + 4$ hydrogen bond distances constrained to the most probable values obtained above (see Figure 2). The residue per turn for Ac−Ala_{24}−NHMe and Act−$Alat_{24}$−NHMe was measured to be 3.6 and 3.7, respectively. To accommodate the longer thio hydrogen bonds, the rise per turn for Act−$Alat_{24}$−NHMe is 0.8 Å longer than that of Ac−Ala_{24}−NHMe (see Table 2).

3_{10}-Helix Structures for Ac−Ala_{10}−NHMe and Act−$Alat_{10}$−NHMe. After equilibration, free molecular dynamics simulations were performed in explicit water to determine the probable conformation of the 3_{10}-helix conformation of

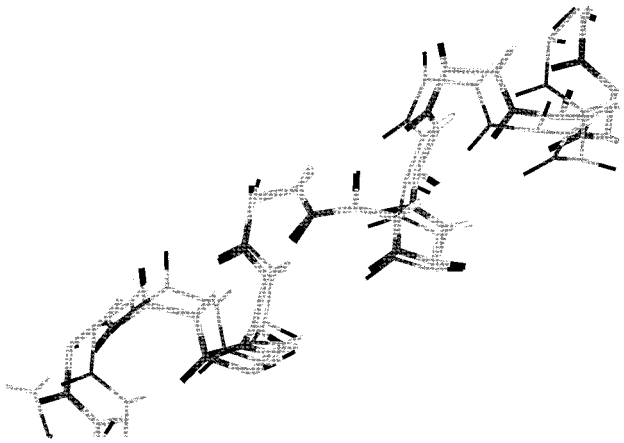

Figure 2. Most probable α_R-helix conformation for Ac−Ala_{24}−NHMe (thinner lines) and Act−$Alat_{24}$−NHMe (thicker lines) obtained by minimization with the ϕ, ψ dihedral angles and the $i \leftarrow i + 4$ hydrogen bond distances restrained to the values obtained from the molecular dynamics simulations. The Act−$Alat_{24}$−NHMe has longer rise per turn. (O and S are 15% gray scaled, C is 40%, N is 70%, and H is 100%).

Ac−Ala_{10}−NHMe and Act−$Alat_{10}$−NHMe. To reduce the bias caused by the C- and the N-terminals, the hydrogen bonds made by the capping group as well as the first and the last two residues are not included in the analysis of the average structure. Consequently, three $i \leftarrow i + 3$ hydrogen bond distances, $3 \leftarrow 6$, $4 \leftarrow 7$, and $5 \leftarrow 8$, and three $i \leftarrow i + 4$ hydrogen bond distances, $3 \leftarrow 7$, $4 \leftarrow 8$, and $5 \leftarrow 9$, were analyzed. Furthermore, only the ϕ, ψ dihedral angles of residues 4−7 were used to calculate the average ϕ and ψ dihedral angles.

The variation of the $i \leftarrow i + 3$ and $i \leftarrow i + 4$ hydrogen bond distances and the ϕ and ψ dihedral angles with simulation time as well as their frequency distributions were plotted (http://www.ludwig.edu.au/archive/tran). For Ac−Ala_{10}−NHMe, the graphs show that while the first 24 ps of the molecular dynamics simulations show the 3_{10}-helical structure, the conformation had changed to a stable α_R-helical structure by the last 16 ps of the calculation. For Act−$Alat_{10}$−NHMe, the 3_{10}-helical conformation remained for 42 ps, after which the 3_{10}-helix conformation also undergoes a transition to the α-helical conformation.

To obtain the (ϕ, ψ) dihedral angles of the 3_{10}-helix conformation for Ac−Ala_{10}−NHMe, a frequency distribution of the (ϕ, ψ) values for the 3_{10} conformation (first 24 ps) of Ac−Ala_{10}−NHMe was analyzed. However, the plot was not smooth, indicating that there was insufficient data. To sample more data, molecular dynamics simulation was performed with flat bottom restraints to ensure that the 3_{10}-helix was not lost during the longer 70 ps simulation. The flat bottom restraints bias the sampling toward $i \leftarrow i + 3$ hydrogen bond distances of less than 2.15 Å. If the distance is above 2.15 Å, a quadratic restraint with a force constant of 100 kcal/mol/Å^2 will be applied to force the distance to be less than or equal to 2.15 Å. The most probable (ϕ, ψ) angles were found to be (−60, −20) (Table 3), which is comparable to the experimentally observed ϕ, ψ dihedral angles for the 3_{10} structure of (−71, −18)[33] given the broad distribution shown in the graph. For Act−$Alat_{10}$−NHMe, a frequency plot of the (ϕ, ψ) values for the 3_{10}-helical conformation (first 42.5 ps) was reasonably smooth, indicating that the sampling was sufficient. The predicted (ϕ, ψ) dihedral angles and $i \leftarrow i + 3$ hydrogen bond distance for Act−$Alat_{10}$−NHMe are (−66, −12) and 2.7 Å, respectively (Table 3).

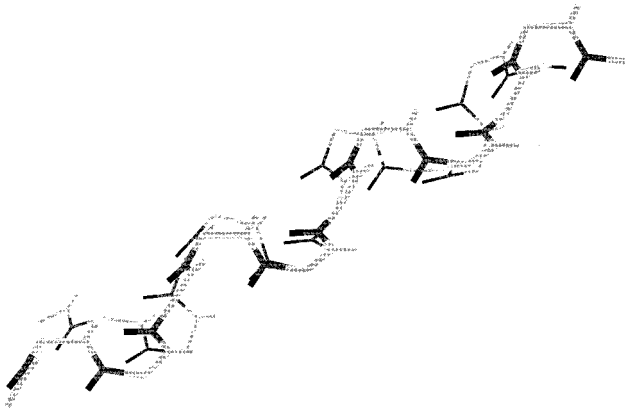

Figure 3. Diagram of the most probable 3_{10}-helical conformation of Ac−Ala_{10}−NHMe (thinner lines) and Act−$Alat_{10}$−NHMe (thicker lines) superimposed on each other. (O and S are 15% gray scaled, C is 40%, N is 70%, and H is 100%).

Table 3. Key Parameters for the 3_{10}-Helix of Ac−Ala_{10}−NHMe and Act−$Alat_{10}$−NHMe Obtained from Molecular Dynamics Simulations

	Ac–Ala_{10}–NHMe	Act–$Alat_{10}$–NHMe
H-bond pattern	$i \leftarrow i + 3$	$i \leftarrow i + 3$
$\phi°$	−60	−66
$\psi°$	−20	−12
H-bond distance (Å)	2.2	2.7
residue/turn	3.1	3.1
rise/turn (Å)	6	6.8

The predicted 3_{10}-helical conformations for Ac−Ala_{10}−NHMe and Act−$Alat_{10}$−NHMe (Figure 3) were obtained by minimization with restraints to those most probable ϕ, ψ dihedral angles and the $i \rightarrow i + 3$ hydrogen bond distances (Figure 3, Table 3). The predicted residue per turn and rise per turn for Ac−Ala_{10}−NHMe (3.1 and 6.0 Å, respectively) are in good agreement with the average of the experimentally obtained values[33] (3.1 and 5.8 Å, respectively). This agreement indicates that the force field and the molecular dynamics method used to predict the 3_{10}-helix conformation are reasonably accurate. To accommodate the longer C═S···H−N hydrogen bonds for Act−$Alat_{10}$−NHMe, the rise per turn for the 3_{10}-helix conformation of Act−$Alat_{10}$−NHMe increases from 6.0 to 6.8 for Act−$Alat_{10}$−NHMe (see Table 3). The number of residue per turn for Act−$Alat_{10}$−NHMe remained the same as that for Ac−Ala_{10}−NHMe (see Table 3).

Relative Free Energy Differences between 3_{10}-Helix and α-Helix for Ac−Ala_{10}−NHMe and Act−$Alat_{10}$−NHMe. Umbrella sampling[50,53] was used to obtain the potential of mean force along the 3_{10}-helix to α-helix pathway and in the reverse direction for both Ac−Ala_{10}−NHMe and Act−$Alat_{10}$−NHMe. The reaction coordinate, λ, for the potential of mean force is defined as the combination of $i \leftarrow i + 3$ and $i \leftarrow i + 4$ hydrogen bond distances (see Figure 1). The probability distributions for the λ values obtained from restrained simulations are shown in Figure 4 with each shade representing each window sampled. The distributions in each window are smooth, indicating that the 100 ps simulation time for each window was sufficient for conformation sampling. The distributions between adjacent windows overlap at high probability regions, indicating that there was sufficient number of windows to cover the transition smoothly.

The relative free energy $A(\lambda)$ was determined for each window to within an additive constant to neighboring windows, the free energy distributions for different windows were overlapped, and the result is shown in Figure 5. Each shade represents each window, and the six points that were used for overlapping adjacent windows are included in the figure. The six points of window overlaps show the relative free energies obtained from the two adjacent windows are consistent with each other, and the quality of the overlaps was sufficient for the calculations.

The forward and backward free energy profiles were overlaid, and the maximum free energy difference between the two profiles is 1 kcal/mol (Figure 6). For Ac−Ala_{10}−NHMe, the average $\Delta A(\alpha \rightarrow 3_{10})$ was 14 kcal/mol, and for Act−$Alat_{10}$−NHMe, the average $\Delta A(\alpha \rightarrow 3_{10})$ was 3.5 kcal/mol. The relative free energies and their decomposition are shown in Table 4. Because of the large uncertainties of the decomposition results, we followed previous authors[51,54] by making only qualitative observations from the decomposition results.

Discussion

Free Energy Difference between the α- and the 3_{10}-Helices of Ac−Ala_{10}−NHMe. The calculated average $\Delta A(\alpha \rightarrow 3_{10})$ for Ac−Ala_{10}−NHMe of 14 kcal/mol is comparable to the 16 kcal/mol calculated by Zhang and Hermans[46] and 10.5 kcal/mol calculated by Tirado-Rives et al.[45] (see Tables 1 and 4). Scheinerman and Brooks[55] improved on the Zimm−Bragg theory by including the 3_{10}-helix as a competing helical state. They showed that the probability for the 3_{10}-helical state relative to the α-helical state increases with decreasing length of peptide. Because our calculations are based on uniform helical structures, the calculated free energy differences between α- and 3_{10}-helices are representative of the long helical segments and, therefore, are an upper bound for the difference that would exist for short helical segments.

The thermodynamic decomposition results (Table 4) indicate that the 3_{10}-helix conformation is disfavored enthalpically by a total $\Delta U = 18.3$ kcal/mol relative to the α-helix conformation. Zhang and Hermans[46] calculated a ΔU of 12 kcal/mol for in vacuo simulation of the Ac−Ala_{10}−NHMe molecule, and Smythe et al.[54] show an increase of up to 7 kcal/mol going from in vacuo to water simulation of Ac−Aib_{10}−NHMe. Hence, the $\Delta U = 18.3$ kcal/mol is indirectly consistent with the values calculated by Zhang and Hermans[46] and Smythe et al.[54] The $\Delta U_{uu-elec}$ and ΔU_{uv-vdw} components favor the 3_{10}-helix conformation, whereas the ΔU_{uu-vdw}, $\Delta U_{uv-elec}$, and $\Delta U_{uu-internal}$ components favored the α-helix conformation. The trend for ΔU_{uu-vdw}, $\Delta U_{uu-elec}$, ΔU_{uv-vdw}, and ΔU_{uv-vdw} are very similar to the values found for Ac−Aib_{10}−NHMe by Smythe et al.[54]

To understand the contributions to the relative free energy difference between α-helical and 3_{10}-helical conformations in water, the differences in dipole moment, hydrogen bond geometry, and the solvent accessible surface area were calculated (Table 5). Taylor et al.[56−58] described three angles that are important for hydrogen bonding in peptide and proteins, N−H···O, in-plane >C═O···H, and out-of-plane >C═O···H.

(53) Leach, A. R. *Molecular Modelling, Principles, and Applications*; Addison-Wesley Longman Limited: England, 1996.

(54) Smythe, M. L.; Huston, S. E.; Marshall, G. R. *J. Am. Chem. Soc.* **1995**, *117*, 5445−5452.

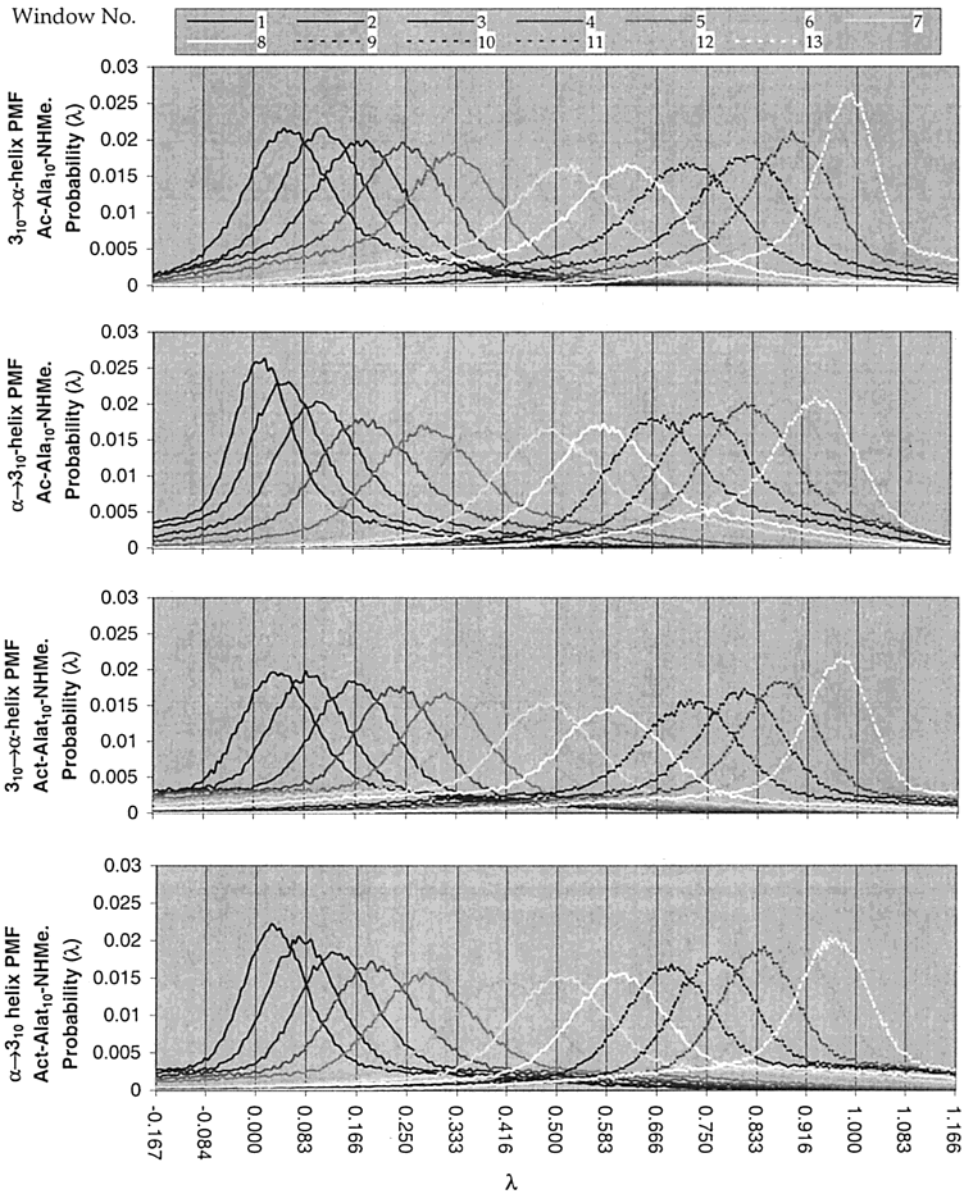

Figure 4. Probability distributions of λ for the transition from a 3_{10}- to α-helix and from an α- to 3_{10}-helix for Ac−Ala_{10}−NHMe and Act−$Alat_{10}$−NHMe. The 13 distributions on each map represent the 13 windows sampled with λ values of 0.000, 0.083, 0.166, 0.250, 0.333, 0.416, 0.500, 0.583, 0.666, 0.750, 0.833, 0.916, and 1.000.

The C═O···H angle in Table 5 is a combination of in-plane >C═O···H and out-of-plane >C═O···H angles.

Three major and opposing factors contributed to the intramolecular enthalpic energy difference (ΔU_{uu}) between the 3_{10}-helix and α-helix. (a) The 3_{10}-helix with $i \leftarrow i + 3$ hydrogen bonds has an extra intramolecular hydrogen bond as compared to the α-helix with $i \leftarrow i + 4$ hydrogen bond. This extra peptide−peptide hydrogen bond contribution precludes the peptide−water interaction and therefore is an in vacuo hydrogen bond. Pauling[59] and Marshall et al.[60] have estimated that the strength of the in vacuo hydrogen bond could be 10 or 12 kcal/mol, respectively. (b) Opposing the extra hydrogen bond that favors the 3_{10}-helical conformation, the 3_{10}-helical conformation is disfavored because the hydrogen bond geometry is not as optimal. The $i \leftarrow i + 4$ hydrogen bond distance for α-helix of 2.1 Å is stronger than the $i \leftarrow i + 3$ hydrogen bond distance for 3_{10}-helix of 2.25 Å. However, the N−H···O and the C═O···H angles for 3_{10}-helix are slightly closer to the optimum angle of 180° and 120°, respectively (see Table 5). Because the hydrogen bond distances appear to be more important than the angles, effectively the α-helix has a better hydrogen bonding geometry than does the 3_{10}-helix. (c) The ΔU_{uu-vdw} component disfavored the 3_{10}-helix conformation by 11.4 kcal/mol. Clark et al.[61] and Hodgkin et

(55) Sheinerman, F. B.; Brooks, C. L. *J. Am. Chem. Soc.* **1995**, *117*, 10098−10103.
(56) Taylor, R.; Kennard, O.; Versichel, W. *J. Am. Chem. Soc.* **1983**, *105*, 5761−5766.
(57) Taylor, R.; Kennard, O.; Versichel, W. *J. Am. Chem. Soc.* **1984**, *106*, 244−248.
(58) Taylor, R.; Kennard, O.; Versichel, W. *Acta Crystallogr., Sect. B* **1984**, *40*, 280−288.
(59) Pauling, L. *The Nature of Chemical Bond*; Cornell University Press: Ithaca, NY, 1960.
(60) Marshall, G. R.; Hodgkin, E. E.; Langs, D. A.; Smith, G. D.; Zabrocki, J.; Leplawy, M. T. *Proc. Natl. Acad. Sci. U.S.A.* **1990**, *87*, 487−491.
(61) Clark, J. D.; Hodgkin, E. E.; Marshall, G. R. In *Molecular Conformation and Biological Interactions*; Balaram, P., Ramaseshan, S., Eds.; Indian Academy of Science: Bangalore, India, 1991; pp 503−510.

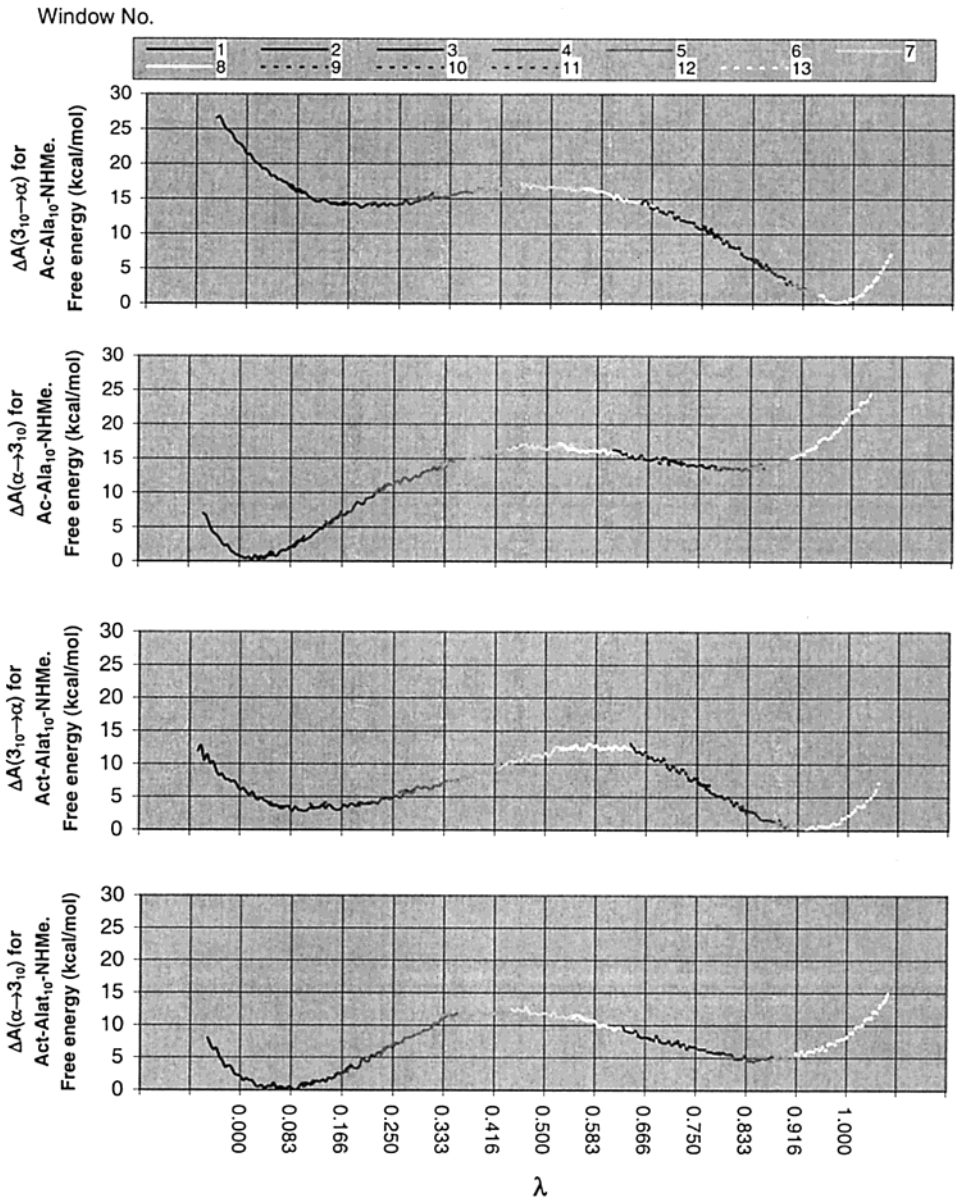

Figure 5. Relative free energy profile for the transition from a 3_{10}- to α-helix and from an α- to 3_{10}-helix for Ac−Ala_{10}−NHMe and Act−$Alat_{10}$−NHMe. The 13 distributions on each map represent the 13 windows sampled with λ values of 0.000, 0.083, 0.166, 0.250, 0.333, 0.416, 0.500, 0.583, 0.666, 0.750, 0.833, 0.916, and 1.000.

al.[62] attributed this to the increase in van der Waals repulsion caused by the unfavorable side-chain stacking in the 3_{10}-helix conformation. The side-chain stacking of 3_{10}-helix is less favorable because they are on identical azimuth positions, whereas they are staggered in the α-helix.

A length dependence on the relative stability of 3_{10}- and α-helix has been suggested by Huston and Marshall,[63] Otoda et al.,[64] and Pavone et al.:[65] the 3_{10}-helix dominates for shorter helical peptides, and the α-helix becomes increasingly favored for longer peptides. This length-dependent preference can be explained by considering the three opposing factors explained in the previous paragraph. The contribution of the extra hydrogen bond favoring the 3_{10}-helix is invariant with length, but the disfavoring of the 3_{10}-helix by the poor hydrogen bond geometry and the side-chain stacking increases with length. 3_{10}-Helix predominates for short peptides because the energy gained by the extra hydrogen bond dominates. With increasing peptide length, α-helix becomes more favorable because the advantage gained by the improved hydrogen bond geometry and the side-chain stacking increases.

Three factors contribute to the difference in peptide−water interactions energy, ΔU_{uv}, between the α- and the 3_{10}-helices: (a) the net dipole moment of the peptide, (b) the solvent accessible surface areas of the peptide, and (c) the $i \leftarrow i + 4$ hydrogen bonded α-helix has three free (not hydrogen bonded) carbonyl groups at the N-terminus and three free N−H groups at the C-terminus. In contrast, the $i \leftarrow i + 3$ hydrogen bonded 3_{10}-helix only has two free groups at each end. The larger solvent accessible surface area of the 3_{10}-helical conformation means more interactions with the solvent (Table 5). Conse-

(62) Hodgkin, E. E.; Clark, J. D.; Miller, K. R.; Marshall, G. R. *Biopolymers* **1990**, *30*, 533−546.
(63) Huston, S. E.; Marshall, G. R. *Biopolymers* **1994**, *34*, 75−90.
(64) Otoda, K.; Yasuyuki, K.; Kimura, S.; Imanishi, Y. *Biopolymers* **1993**, *33*, 1337−1345.
(65) Pavone, V.; Di, B. B.; Santini, A.; Benedetti, E.; Pedone, C.; Toniolo, C.; Crisma, M. *J. Mol. Biol.* **1990**, *214*, 633−635.

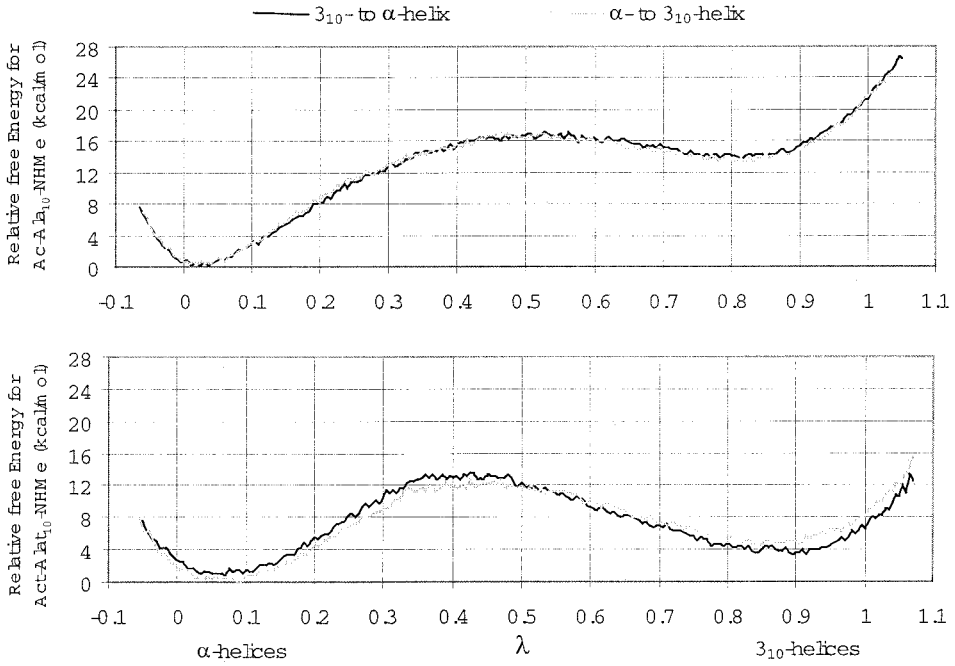

Figure 6. To examine the reproducibility of the forward and reverse run, the relative free energy profile of 3_{10}- → α-helix PMF was inverted and superimposed on results for the α- → 3_{10}-helix PMF. (a) Ac−Ala_{10}−NHMe and (b) Act−$Alat_{10}$−NHMe. The α-helix is at the minimum near $\lambda = 0.083$, and the 3_{10}-helix is at the minimum near $\lambda = 0.916$.

Table 4. Decomposition of $\Delta A(\alpha \rightarrow 3_{10})$ into ΔU and $-T\Delta S$ Components for Ac−Ala_{10}−NHMe and Act−$Alat_{10}$−NHMe

				peptide–peptide components of ΔU				peptide–water components of ΔU		
	ΔA	ΔU	$-T\Delta S$	Coulombic	van der Waals	nonbonded	internal	Coulombic	van der Waals	nonbonded
Ac−Ala_{10}−NHMe	14 ± 3.9^a	18.3 ± 22.5^a	-4.3 ± 26.4^b	-14.0 ± 7.9^a	11.4 ± 8.9^a	-2.5 ± 11.6^a	5.1 ± 17.5^a	23.0 ± 18.1^a	-7.2 ± 8.8^a	15.7 ± 18.0^a
Act−$Alat_{10}$−NHMe	3.5 ± 1.7^a	15.5 ± 23.9^a	-12 ± 25.6^b	-22.4 ± 6.4^a	17.9 ± 9.8^a	-4.5 ± 10.3^a	3.2 ± 15.7^a	26.5 ± 21.6^a	-9.6 ± 9.2^a	16.8 ± 20.9^a
differences	-10.5 ± 5.8^b	-2.8 ± 46.4^b	-7.7 ± 52.0^b	-8.4 ± 14.3^b	6.5 ± 18.7^b	-2.0 ± 21.9^b	-1.9 ± 33.2^b	3.5 ± 39.7^b	-2.4 ± 18.0^b	1.1 ± 38.9^b

[a] Uncertainties were obtained from 1 standard deviation of the sample. [b] Uncertainties were obtained from standard error propagation where the uncertainty of a sum is the sum of the uncertainties.

Table 5. Comparison of Dipole Moment, Hydrogen Bond Geometry, and Accessible Surface Area between the α-Helical and the 3_{10}-Helical Conformations of Ac−Ala_{10}−NHMe and Act−$Alat_{10}$−NHMe[a]

	Ac–Ala_{10}–NHMe				Act–$Alat_{10}$–NHMe			
	α-helix-3_{10}-helix		3_{10}-helix-α-helix		α-helix-3_{10}-helix		3_{10}-helix-α-helix	
	α-helix	3_{10}-helix	α-helix	3_{10}-helix	α-helix	3_{10}-helix	α-helix	3_{10}-helix
dipole moment (debye)	36 ± 0.6	31 ± 0.9	36 ± 0.6	31 ± 1.1	63 ± 0.7	61 ± 1.0	62 ± 0.8	61 ± 1.0
$i \leftarrow i + 3$ hydrogen bond distances (Å)	3.0 ± 0.2	2.2 ± 0.2	3.0 ± 0.2	2.3 ± 0.2	3.2 ± 0.2	2.7 ± 0.2	3.1 ± 0.2	2.7 ± 0.2
$i \leftarrow i + 4$ hydrogen bond distances (Å)	2.1 ± 0.2	4.5 ± 0.2	2.1 ± 0.2	4.5 ± 0.2	2.7 ± 0.2	5.1 ± 0.2	2.7 ± 0.2	5.2 ± 0.2
C═O...H or C═S...H angles (deg)	149 ± 9	129 ± 9	148 ± 9	128 ± 9	132 ± 7	113 ± 7	132 ± 0.2	113 ± 7
N−H...O or N−H...S angles (deg)	157 ± 11	163 ± 10	156 ± 11	163 ± 10	144 ± 13	158 ± 12	144 ± 13	158 ± 11
solvent accessible area (Å^2)	604 ± 10	682 ± 11	604 ± 10	681 ± 11	661 ± 9	733 ± 10	660 ± 10	730 ± 11

[a] The values are calculated for each of the four free energy profiles, α- to 3_{10}-helices and 3_{10}- to α-helices for both Ac−Ala_{10}−NHMe and Act−$Alat_{10}$−NHMe. The uncertainties are equivalent to 1 standard deviation from the mean.

quently, the 3_{10}-helical conformation is favored at both the $\Delta U_{uv-elec}$ and the ΔU_{uv-vdw} components (see Table 4). This qualitatively accounts for a ΔU_{uv-vdw} of −7.2 kcal/mol. However, the decrease in dipole moment and the decrease in free carbonyl oxygen and NH groups disfavor the 3_{10}-helical conformation, especially for the $\Delta U_{uv-elec}$ component. This qualitatively explains the large $\Delta U_{uv-elec}$ of 23 kcal/mol.

Table 4 also shows that entropically, 3_{10}-helix is favored by −4.3 kcal/mol relative to the α-helix. This is consistent with the in vacuo result −4 kcal/mol for Ac−Ala_{10}−NHMe calculated by Zhang and Hermans.[46] The Smythe et al.[47,54] result for Ac−Aib_{10}−NHMe also shows a similar trend, −4.3 in vacuo and −4 in water. Normal-mode analysis by Basu[66] also gave a similar result. Huston and Marshall[63] suggested that this entropic favoring of the 3_{10}-helix for polyAib was due to it being longer and thinner.

Free Energy Difference between the α- and the 3_{10}-Helices of Act−$Alat_{10}$−NHMe. The $\Delta A(\alpha \rightarrow 3_{10})$ for Act−$Alat_{10}$−NHMe is 3.5 kcal/mol, 10.5 kcal/mol smaller than the value for Ac−Ala_{10}−NHMe (Table 4). The Act−$Alat_{10}$−NHMe 3_{10}-helix is disfavored enthalpically by 15.5 kcal/mol as compared to 18.3 kcal/mol for Ac−Ala_{10}−NHMe; however, the Act−$Alat_{10}$−NHMe 3_{10}-helix is favored entropically by 12 kcal/mol as compared to 4.3 kcal/mol for Ac−Ala_{10}−NHMe.

(66) Basu, G.; Kitao, A.; Hirata, F.; Go, N. *J. Am. Chem. Soc.* **1994**, *116*, 6307−6315.

Contrary to the total peptide−peptide energy, $\Delta U_{uu-total}$ for Ac−Ala$_{10}$−NHMe which disfavored 3_{10}-helix by 2.6 kcal/mol, the $\Delta U_{uu-total}$ for Act−Alat$_{10}$−NHMe favored the 3_{10}-helical conformation by 1.3 kcal/mol. The $\Delta U_{uu-total}$ for Ac−Ala$_{10}$−NHMe was explained earlier in terms of three factors: 3_{10}-helix is favored by the extra hydrogen bond, it is disfavored because of a poorer hydrogen bond geometry, and unfavorable side-chain stacking. The number of hydrogen bonds is independent of the thio substitution; however, the 3_{10}-helix geometry for Act−Alat$_{10}$−NHMe has a hydrogen geometry (2.7 Å) that is as good as the hydrogen bond geometry (2.7 Å) for α-helix (Table 5). The number of residues per turn (Table 3) shows that the side-chain stacking in the thio substituted 3_{10}-helical conformation is the same as that in the α-helix. However, the side chains are further away because of the longer rise per turn; therefore, disfavoring of the 3_{10}-helix in Ac−Ala$_{10}$−NHMe is partly relieved by thio substitution. The combined effect of these three factors qualitatively explains the decrease in $\Delta U_{uu-total}$ from 2.6 kcal/mol in Ac−Ala$_{10}$−NHMe to −1.3 kcal/mol for Act−Alat$_{10}$−NHMe.

The $\Delta U_{uv-nonbond}$ component is 16.8 kcal/mol for Act−Alat$_{10}$−NHMe, very similar to the 15.7 kcal/mol of Ac−Ala$_{10}$−NHMe (see Table 4). The change in surface area, Δsurfacearea-(α → 3_{10}), for Ac−Ala$_{10}$−NHMe is 78 Å^2 (Table 5), favoring the 3_{10}-helix. Thio substitution changed this Δsurfacearea(α → 3_{10}) to 71 Å^2 (Table 5), still favoring the 3_{10}-helix but to a lesser degree. The Δdipole(α → 3_{10}) for Ac−Ala$_{10}$−NHMe is −5 D (Table 5), disfavoring the 3_{10}-helix. Thio substitution changed the Δdipole(α → 3_{10}) to −1 or −2 D, still disfavoring the 3_{10}-helix but to a lesser extent than in the polyalanine. The number of non-hydrogen bonded carbonyl and NH groups remained similar with thio substitution; however, the effective "hydrogen bond" with water is less, thus still disfavoring 3_{10}-helix but to a lesser extent. The combined effect of these three factors contributes to the increase in $\Delta U_{uv-nonbond}$(α → 3_{10}) from 15.7 kcal/mol in Ac−Ala$_{10}$−NHMe to 16.8 kcal/mol for Act−Alat$_{10}$−NHMe.

Entropy is examined qualitatively by considering the number of conformations with different (ϕ, ψ) values in a molecular dynamic simulation of the 3_{10}-helix or α-helix. This number of conformations with different (ϕ, ψ) values is plotted against the percentage of the total number of conformations, from the most probable to the least probable conformation in the trajectories (Figure 7). When 90% of all conformations are sampled, the Ac−Ala$_{10}$−NHMe α-helix has 345 different conformations, and the 3_{10}-helix has a much larger 436 conformations. This trend exists not just at 90% of all conformations but throughout the % distribution space. Therefore, the 3_{10}-helix of Ac−Ala$_{10}$−NHMe is more flexible and thus favored entropically. A similar argument also leads to the conclusion that the 3_{10}-helix of Act−Alat$_{10}$−NHMe is more flexible and therefore is stabilized entropically when compared to the α-helical conformation. This is consistent with a previous report,[63] which attributes the entropic favoring of 3_{10}-helix over α-helix to 3_{10}-helix being longer and thinner.

Relative to the α-helix, the 3_{10}-helix of Ac−Ala$_{10}$−NHMe is favored entropically by 4.3 kcal/mol (the value for $T\Delta S$ is used instead of ΔS). The 3_{10}-helix of Act−Alat$_{10}$−NHMe is favored over the α-helix entropically by a larger amount (12 kcal/mol, Table 4). This result is consistent with Figure 7 where the differences in the number of conformations for the α-helix and the 3_{10}-helix for polythioalanine are usually bigger than that for polyalanine. The α-helix conformation of Act−Alat$_{10}$−NHMe has the bulkier sulfurs and is less able to move in the packed α-helix conformation. This leads to fewer α-helix conformations for Act−Alat$_{10}$−NHMe (Figure 7). Therefore, a contribution to the increase of entropy favoring the 3_{10}-helix upon thio substitution is not the increase in entropy of the 3_{10}-conformation, but the decrease in entropy of the α-helix conformation.

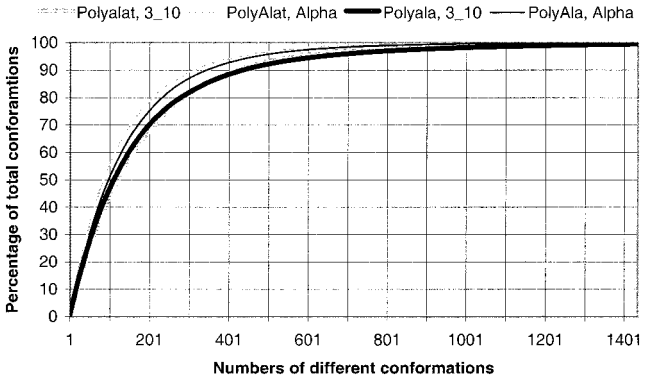

Figure 7. Entropy is qualitatively examined by looking at the number of different conformations which a hydrogen bonded 3_{10}-helix or α-helix can make. The *y*-axis represents the percentage of conformations, from the most probable to the least probable. The *x*-axis represents the number of different conformations. The conformations in a trajectory centering on the α- or 3_{10}-helix were put into conformational bins, and the bins were sorted according to frequencies. From the most popular to the least popular bins, the percentage of the total conformation (*y*-axis) and the number of different conformations (*x*-axis) were evaluated. At a certain percentage, this distribution shows the number of accessible conformation and consequently the relative flexibility of the 3_{10}-helix or the α-helix for Ac−Alat$_{10}$−NHMe and Act−Alat$_{10}$−NHMe.

Conclusions

Our molecular dynamic simulations show that the most prominent structural change to the α_R- and 3_{10}-helix conformations introduced by the thio substitution is the increased hydrogen bond distance from 2.1 to 2.7 Å. Consequently, the ϕ and ψ dihedral angles and the rise per turn of the α_R- and 3_{10}-helix conformations change to accommodate for the longer C═S···H−N hydrogen bond. The most prominent stability change is the decrease in the ΔA(α → 3_{10}) from 14 to 3.5 kcal/mol upon thio substitution.

To understand the effect of thio substitution upon the relative stability of the α_R- and 3_{10}-helix conformations, the ΔA(α → 3_{10}) for Ac−Ala$_{10}$−NHMe and Act−Alat$_{10}$−NHMe was decomposed. The ΔU_{uu} component was explained in terms of the extra 3_{10}-helix hydrogen bond, the hydrogen bond geometry for the 3_{10}- and α-helix conformation, and the side-chain stacking in the 3_{10}-helix conformation. The ΔU_{uv} component was explained by the higher surface area for the 3_{10}-helix, the lower dipole of the 3_{10}-helix, and the fewer free carbonyl and NH groups for the 3_{10}-helix. The entropy favoring of the 3_{10}-helix conformation by 4.3 kcal/mol is because the hydrogen bonded 3_{10}-helix conformation can adopt more conformations (more flexible) relative to the α-helix. Upon thio substitution, this differential flexibility is even more apparent because the α-helix conformation of Act−Alat$_{10}$−NHMe is even less flexible. In addition to the increased resistance to enzymatic degradation property of thiopeptides, the elongated α- and 3_{10}-helical structures and the altered relative stability suggest that thiopeptides will be potentially useful building blocks for drug design and protein engineering.

JA011916O